A new look at stellar outows: Spitzer observations of the Herbig-Haro 46/47 system

Noriega-Crespo, A.; Morris, P.; Marleau, F.R.; Dishoeck, E.F. van

The Astrophysical Journal Supplement Series, 154:352–358, 2004 September

A NEW LOOK AT STELLAR OUTFLOWS: *SPITZER* OBSERVATIONS OF THE HH 46/47 SYSTEM

Alberto Noriega-Crespo,[1] Patrick Morris,[1] Francine R. Marleau,[1] Sean Carey,[1] Adwin Boogert,[2] Ewine van Dishoeck,[3] Neal J. Evans II,[4] Jocelyn Keene,[1,5] James Muzerolle,[6] Karl Stapelfeldt,[5] Klaus Pontoppidan,[3] Patrick Lowrance,[1] Lori Allen,[7] and Tyler L. Bourke[8]

Received 2004 March 26; accepted 2004 May 13

ABSTRACT

We present the Early Release Observations of the HH 46/47 system and HH 46 IRS 1 source, taken with the three instruments aboard the *Spitzer Space Telescope*. The optically invisible southwest lobe, driven by the HH 47C bow shock, is revealed in full detail by the Infrared Array Camera (IRAC) images and displays a "loop"-like morphology. Both of the mid-infrared outflow lobes are narrower than those of CO flow. We believe that the combination of emission by H_2 rotational lines [$S(11)$–$S(4)$] and some atomic lines, which fall within the IRAC passbands, are responsible for the bulk of the observed emission, although contributions from the 3.3, 6.2, and 7.7 μm polycyclic aromatic hydrocarbon emission bands cannot be ruled out. Weak spectral features corresponding to these emitters are present in the Infrared Spectrograph spectrum of the HH 47A bow shock. The spectrum of HH 46 IRS 1 shows remarkable similarities to those of high-mass protostars, which include the presence of H_2O, CO_2, CH_4, and possibly NH_3, CH_3OH, and NH_4^+ ices. The high ice abundances and the lack of signs of thermal processing indicate that these ices in the envelope are well shielded from the powerful outflow and its cavity. Emission from the Bok globule at 24 μm is detected and displays a similar structure to that observed at 8 μm.

Subject headings: infrared: ISM — ISM: Herbig-Haro objects — ISM: individual (HH 46–47) — ISM: jets and outflows — ISM: molecules — stars: formation

1. INTRODUCTION

Jets and outflows arising from young stellar objects are some of the most spectacular signatures of the early stages of the low-mass star formation process. A handful of these objects, because of their brightness at optical and near-infrared wavelengths, are considered archetypes of their class, and the HH 46/47 system belongs to this group. The HH 46/47 outflow is found in an isolated Bok globule (ESO 210-6A; Schwartz 1977) and since its discovery has been the subject of several studies to understand its shock physics and chemistry as well as the dynamical evolution of the outflow and its driving source, HH 46 IRS 1 (IRAS 08242−5050; Raymond et al. 1994; Correira 2000; Schwartz & Greene 2003). The source is classified as a very young Class I protostellar object and has a bolometric luminosity of $\sim$12 $L_\odot$ (Adams et al. 1987; Emerson et al. 1984). At a distance of 450 pc (Heathcote et al. 1996), the projected extent of the brightest knots, from the blueshifted bow shock HH 47D to the redshifted HH 47C bow shock, is 0.57 pc. Recent deep Hα and S II 6717 Å images show two larger bow shocks aligned with the flow's axis and separated by $\sim$2.6 pc (Stanke et al. 1999). The presence of multiple bow shocks strengthens the idea of a time-dependent ejection mechanism from HH 46 IRS 1 and reveals HH 46/47 as a parsec-size outflow. Proper-motion and radial velocity measurements in the optical and near-infrared imply flow velocities of $\sim$300 km s^{-1} (Dopita et al. 1982; Reipurth & Heathcote 1991; Eislöffel & Mundt 1994; Micono et al. 1998) and an orientation of $\sim$35° of the outflow axis with respect to the plane of the sky. From optical spectroscopic observations and comparison with shock models, shock velocities of $\sim$35–70 km s^{-1} have been inferred (Morse et al. 1994). Collisional excitation is the main emission mechanism in HH objects, and this is the case for HH 46/47, although H_2 fluorescence has been observed in HH 47A (Curiel et al. 1995).

HH 46/47 was selected as a target for *Spitzer* observations because of its spectacular morphology at optical wavelengths and its relatively unusual outflow characteristics as traced by the H_2 near-infrared emission at 2.12 μm (Eislöffel et al 1994). In this paper, we present new results on the morphology of the outflow, the spectra of its deeply embedded source, and the HH 47A bow shock.

2. OBSERVATIONS

All the data were obtained with the *Spitzer Space Telescope* during Science Verification period. HH 46/47 was observed using the Multiband Imaging Photometer for *Spitzer* (MIPS; Rieke et al. 2004) on 2003 November 19, the Infrared Array Camera (IRAC; Fazio et al. 2004) on November 21, and the Infrared Spectrograph (IRS; Houck et al. 2004) on November 23. The MIPS observations were performed in its photometry mode

[1] *Spitzer* Science Center, California Institute of Technology, MC 220-6, Pasadena, CA 91125.
[2] Department of Astronomy, California Institute of Technology, MC 105-24, Pasadena, CA 91125.
[3] Leiden Observatory, University of Leiden, P.O. Box 9513, 2300 RA Leiden, Netherlands.
[4] Department of Astronomy, University of Texas at Austin, 1 University Station C1400, Austin, TX 78712-1083.
[5] Jet Propulsion Laboratory, California Institute of Technology, 4800 Oak Grove Drive, Pasadena, CA 91109.
[6] Steward Observatory, University of Arizona, 933 North Cherry Avenue, Tucson, AZ 85721.
[7] Harvard-Smithsonian Center for Astrophysics, 60 Garden Street, Cambridge, MA 02138.
[8] Harvard-Smithsonian Center for Astrophysics, Submillimeter Array Project, P.O. Box 824, Hilo, HI 96720.

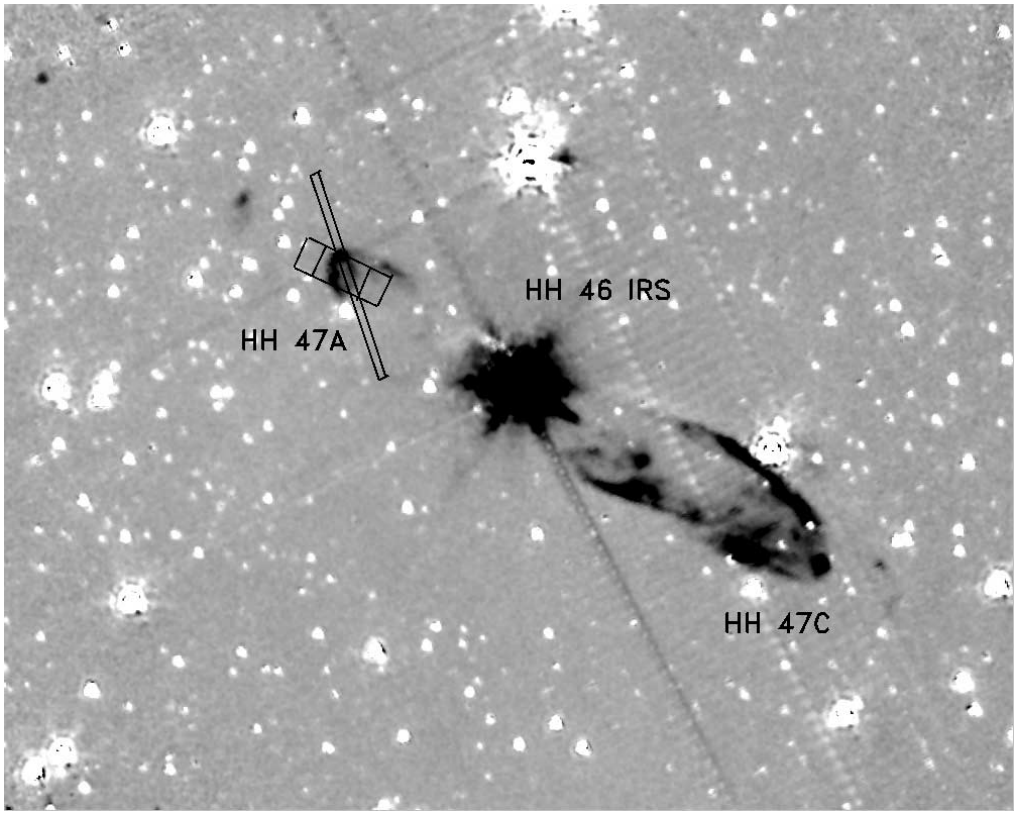

FIG. 2.—HH 46/47 IRAC difference image using channels 2 (4.5 μm) minus 1 (3.6 μm). Essentially everything dark along the outflow is due to H_2 emission. Near the source, a faint white feature traces the scattered light from the cavity, a well-recognized feature at optical wavelengths. The image shows the IRS slit schematic positions for the SL first-order and LH first pointing on the HH 47A bow shock. The same setup and slit orientation were used on the HH 46 IRS source. The map shows a $5' \times 5'$ field. North is up, and east is to the left.

and only at 24 μm with 3 s frames and a total integration time of 155.2 s. The IRAC observations used high dynamic range 30 s frames with an on-source time of 330 s. The IRS observations were taken at the HH 46 IRS source and HH 47A bow shock. The main goal of the spectroscopic observations was to obtain a high signal-to-noise ratio (>100) spectrum of the *IRAS* source over the 5.5–37 μm wavelength range. For the HH 47A bow shock, the integration times were adjusted to reach a signal-to-noise ratio of $\sim$10 over the same wavelength range. Therefore, the IRS on-source times were 243 s at shorter (Short-Low [SL] and Short-High [SH])[9] and 75 s at longer (Long-High [LH]) wavelengths for HH 46 IRS, and 121 s (SL and SH) and 63 s (LH) for HH 47A, respectively. The data from the three instruments were processed with the *Spitzer* Science Center pipeline S9.5,[10] which provides the basic calibrated data, the starting point for further analysis.

3. RESULTS AND DISCUSSION

3.1. *The IRAC Mid-Infrared Morphology*

The HH 46/47 outflow is shown in Figure 1 (Plate 1), which is a composite image of the four IRAC bands. The clear definition of the counterlobe, similar to a loop, which joins the HH 47C bow shock with the source, is perhaps the most remarkable feature of this picture. One could argue that most of the brightest regions in this picture have been detected in the near-infrared in the H_2 images at 2.12 μm (Eislöffel et al. 1994); however, for the first time we have the complete picture of the outflow at 3.6–8 μm. The southwest "loop" driven by the HH 47C bow shock (Fig. 2) has an extent of $2'$ and a maximum width of $\sim 36''$. The blueshifted lobe is nearly half this size, with a $1'.3$ length and a $12''$ width. These scales are not very different from those of the CO $J = 1$–2 outflow (Chernin & Masson 1991; Olberg et al. 1992). Based on $\sim 20''$ beam observations, the CO outflow shows a fully developed redshifted lobe with an extent of $2'$ and a width of $\sim 1'$. The blueshifted CO lobe is once again nearly half the size of its counterpart and ends sharply at the boundary of the Bok globule. This asymmetry in the sizes of the lobes is usually explained by the presence (redshifted lobe) and absence (blueshifted lobe) of molecular gas that can be entrained by the outflow. The IRAC observations place HH 46/47 well within the CO outflow and are consistent with the idea that the atomic/ionic jet is the main driver of the flow (e.g., Raga & Cabrit 1993). The estimates of the amount of swept-up ambient gas ($\sim 0.05\ M_\odot$) and the necessary mechanical luminosity to move it ($\sim 0.5 \times 10^{-2}\ L_\odot$), using the H_2 2.12 μm and CO $J = 2$–1 emission, are nearly identical (Eislöffel et al 1994). Unfortunately, it is very difficult to perform a similar comparison using the IRAC channels, because they include many emission lines and broad spectral features. In a companion paper (Raga et al. 2004), we carried out detail hydrodynamical simulations of a jet evolving into an ambient medium that mimics that of a Bok globule. The simulations considered two of the most common scenarios for the formation of low-mass stellar outflows, the "*X*-wind model" (i.e., latitude-dependent wind; Shu et al. 1995) and the "standard

[9] See http://ssc.spitzer.caltech.edu/documents.
[10] See http://ssc.spitzer.caltech.edu/postbcd.

model" (i.e., a collimated jet without precession). Both models can reproduce the global properties of the HH 46/47 outflow.

As mentioned above, the IRAC channels are relatively broad, and therefore, they include several fine-structure atomic and H_2 molecular lines, which are known to arise in low-mass outflows (Cabrit et al. 1999; Rosenthal et al. 2000; Noriega-Crespo 2002; Nisini 2003; Lefloch et al. 2003). For low-velocity shocks, as those inferred in HH 46/47 (30–70 km s^{-1}), atomic emission lines like Brα and Ar II 6.99 μm could be present, as well as several H_2 vibrational transitions and the head of the CO emission band (4.6–4.8 μm). Certainly some of the brightest emission lines at these wavelengths correspond to rotational H_2 transitions (Molinari et al. 2000; Moro-Martin et al. 2001; Molinari & Noriega-Crespo 2002). For the typical conditions associated with low-mass outflows, with excitation temperatures ranging from $\sim$500 to 2000 K, the $S(11)$ at 4.18 μm through $S(4)$ at 8.02 μm lines can be several times brighter than the classical H_2 diagnostic line at 2.12 μm (Kaufman & Neufeld 1996). Furthermore, IRAC channels 3 and 4 are well suited to detect the broad polycyclic aromatic hydrocarbon (PAH) emission features at 6.2 and 7.7 μm. One way to illustrate this relative contribution from H_2 and PAH emission is to compare the "PAH-free" band channel 2 at 4.5 μm with channel 1 at 3.6 μm, where the PAH emission comes mostly from the 3.3 μm feature, which is weaker than those at longer wavelengths. Figure 2 shows the difference between channels 2 and 1; essentially, the Bok globule emission (the reddish translucent color in Fig. 1) disappears around the outflow. We suspect that the rest of the emission in Figure 2 is very likely molecular H_2 and CO and also that the PAH contribution to the emission from the outflow walls is small. This last assertion is partially supported by the IRS spectrum of HH 47A, where in some of the slit positions light from the cavities is observed (Fig. 2).

In the scenario in which an atomic/ionic jet pierces through the maternal molecular cloud and drives a molecular outflow, one expects the dust to be dragged along with the gas, and one should be able to detect a "dust cavity" surrounding the flow; this idea motivated the 24 μm observations. Unfortunately, the HH 46 IRS 1 source is 3.9 Jy at 24 μm and nearly saturates the array in the 3 s photometric observations. Figure 3 shows the 24 μm image around HH 46/47; the central source is too bright and engulfs within its point-spread function the central region around the outflow. Emission near HH 47A and 47C is detected at 24 μm (Fig. 4 [Plate 2]) and is likely to arise at the bow shocks. Figure 4 also shows how the southwest outflow lobe is disrupting the Bok globule and that *Spitzer* is able to detect the faint dust continuum emission at 24 μm, which shows a similar structure to that observed with IRAC at 8 μm.

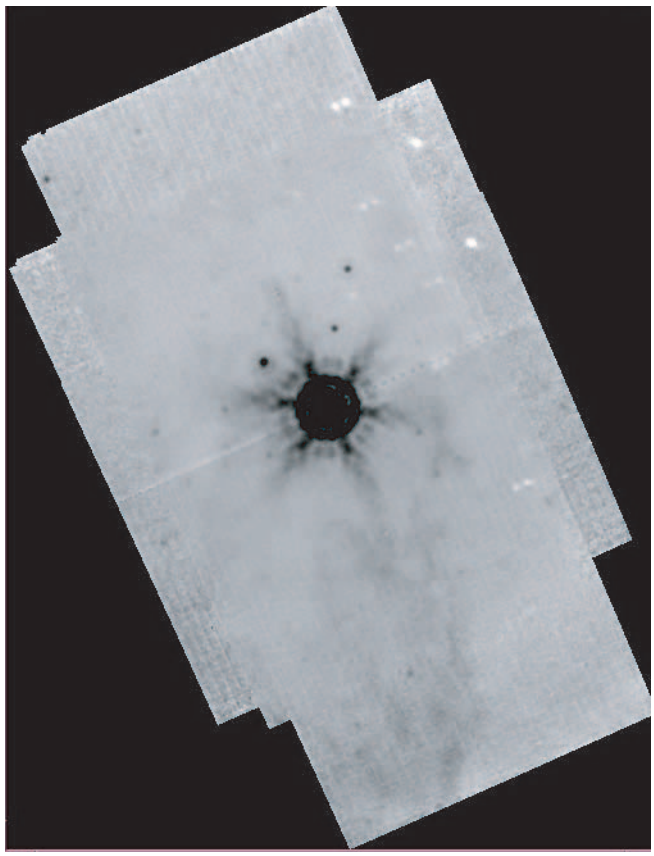

FIG. 3.—HH 46/47 MIPS 24 μm image. The bright HH 46 IRS 1 source (3.9 Jy) dominates the region around the outflow; however, some of the Bok globule emission is clearly detected. The map shows a $7' \times 12.'5$ field. North is up, and east is to the left.

3.2. *The Mid-Infrared Spectrum of HH 46 IRS 1 and HH 47A*

In Figure 5, the IRS spectrum toward HH 46 IRS 1 is presented. It is a composite of the low-resolution ($R = \lambda/\Delta\lambda \approx 64$) data from 5–10 μm and the high-resolution ($R \approx 600$) spectrum from 10–37 μm. The 5–20 μm section of the spectrum shows a steeply rising continuum characteristic of a deeply embedded protostellar object surrounded by a thick envelope. A rich spectrum of ice and silicate absorption features is superposed, reminiscent of high-mass protostars such as W33A (Gibb et al. 2004). The low-resolution 5–10 μm portion of the spectrum is covered with a blend of absorption features.

The 7.67 μm band due to solid CH_4 is clearly detected, as are the 6.0 and 6.85 μm broad absorption bands. The latter features themselves are a blend of absorption transitions of a number of different molecules. At the H_2O column density derived from the 3.0 μm band (8.0×10^{18} cm^{-2}; Boogert et al. 2004), the H_2O bending mode contributes 50% to the 6.0 μm band. Admixtures of other molecules such as HCOOH or H_2CO in the blue wing and carbonaceous material in the red wing (Schutte et al. 1996; Keane et al. 2001) must contribute significantly. A decomposition of this band is complicated by the low spectral resolution, although even at higher resolution such decomposition is not trivial. The main carrier of the prominent 6.85 μm band is not yet firmly identified, although NH_4^+ is a plausible candidate (Schutte & Khanna 2003) and CH_3OH contributes only 10%, when the column density derived from ground-based observations is used (Boogert et al. 2004). Keane et al. (2001) have shown that the 6.85 μm profile shifts in position with temperature of the source. For HH 46 IRS 1, the position is consistent with that found in the coldest high-mass sources. Even within the deep 9.7 μm silicate band, individual absorption substructures are visible. Analysis of these features awaits a characterization of the intrinsic profile of the silicate band. The sharp feature at the bottom of the silicate band may well be due to solid CH_3OH. An inflection around 9.0 μm could be due to NH_3 ices. Alternatively, it could be caused by a different ratio of pyroxenes to olivines in this source, with possibly a higher degree of aluminum-containing silicates (Demyk et al. 1999; Kemper et al. 2004). There is no hint of any sharp feature at 11.3 μm caused by crystalline silicates such as forsterite. A shallow broad feature at 11.2 μm could be due to absorption by aromatic species

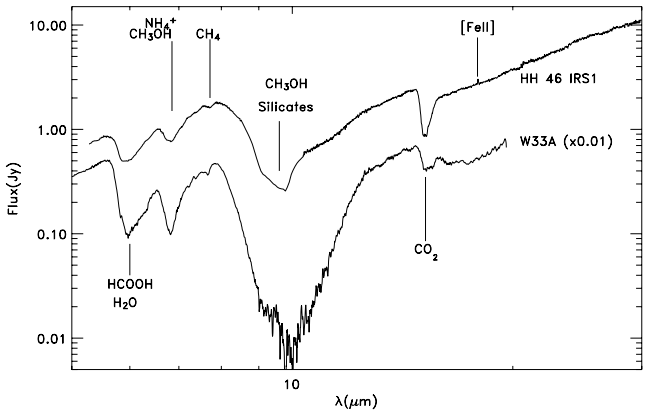

FIG. 5.—IRS spectrum of the HH 46 IRS 1 source (*upper line*) compared with that of W33A (*lower line*), a high-mass protostar (Gibb et al. 2000), scaled down by a factor of 100.

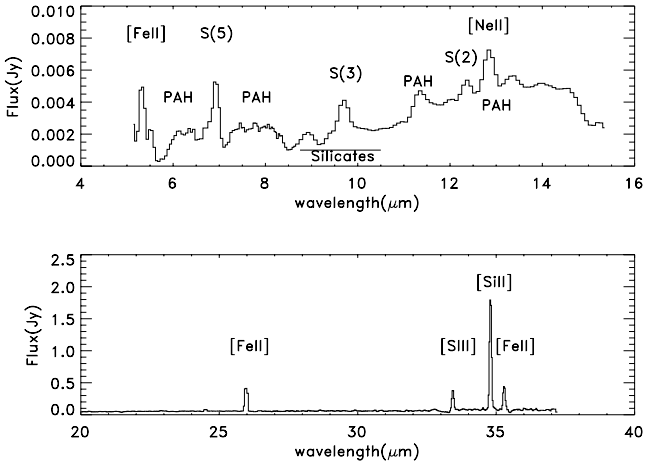

FIG. 6.—IRS spectrum of the HH 47A bow shock from 5 to 14 μm (*top*) and from 20 to 37 μm (*bottom*).

(Bregman et al. 2000). The broad shoulder at 12–14 μm can almost certainly be ascribed to the libration mode of amorphous H_2O ice. Finally, the dominant absorption feature longward of the 9.7 μm silicate band is that due to solid CO_2 at 15.2 μm. The solid CO_2 band profile in this high-resolution portion of the spectrum is analyzed in detail in conjunction with ground-based L- and M-band spectra in the accompanying paper by Boogert et al. (2004). It appears that this band traces unprocessed, amorphous ices and thus that the ices in the envelope surrounding HH 46 IRS 1 are relatively pristine. This is further emphasized by the high ice abundance. At a molecular hydrogen column density of $(3-6)\times10^{22}$ (Boogert et al. 2004), the H_2O abundance of $\sim10^{-4}$ is high and comparable to massive protostars. In fact, the CH_4 and CO_2 ratios of 4% and 30% with respect to water are a factor of 2 larger compared to high-mass objects. Overall, the ice abundances and the ice band profiles indicate that the line of sight toward HH 46 is very cold and ice-rich. Given the strong outflow activity of the source highlighted by our IRAC data, this lack of evidence for heating is surprising but emphasizes the importance of geometry in analyzing low-mass protostellar environments.

The spectrum of HH 47A is dominated by bright atomic/ionic forbidden emission lines between 25 and 37 μm, with peak intensities ranging from 0.5 to 2.5 Jy (e.g., [Fe II] 24.51 μm, [Fe II] 25.98 μm, [S III] 33.5 μm, [Si II] 34.8 μm, and [Fe II] 35.35 μm). These lines are not surprising at the bow shock based on the inferred shock velocities, as high as 70 km s^{-1}, and are consistent with the optical ground-based spectroscopic measurements. At shorter wavelengths (<15 μm), the spectrum is remarkably different (Fig. 6) and is very likely sampling a distinct region, perhaps the interface between the bow shock and the cavity or the cavity itself (see Fig. 2). The spectrum shows a handful of faint (<8 mJy) H_2 lines [*S*(5), *S*(3), and *S*(2)] blended or superposed with a continuum made mostly by broad PAH features modified at 10 μm by silicate absorption. The excitation temperature derived from these lines is 1140 ± 150 K, which is quite similar to what is measured in some embedded outflows; however, the column density is $\sim4.6\times10^{14}$ cm^{-2}, several orders of magnitude smaller than commonly measured (Moro-Martin et al. 2001). This result is consistent with a very thin layer of collisionally excited H_2 (10^{10}–10^{11} cm for gas densities of $\sim10^4$ cm^{-3}). The [Ne II] 12.8 μm emission line probably originates at the bow shock, since shock velocities of $\sim$60 km s^{-1} are required to excite it and are enough to dissociate molecular hydrogen (Cabrit et al. 1999; Lefloch et al. 2003).

4. SUMMARY

1. IRAC observations of the HH 46/47 system have shown with unprecedented clarity the structure of the HH 47C southwest outflow lobe, and revealed a more subtle and complex morphology than expected, based just on optical and near-infrared images. We suspect that the bulk of the emission arising from the loops or cavities is due to H_2 pure rotational lines, with perhaps some contribution of warm small dust particles. Despite its striking morphology, numerical simulations of HH 46/47, using either an *X*-wind or standard jet model, can reproduce its overall features (Raga et al. 2004).

2. The MIPS 24 μm emission from the outflow is overwhelmed by the light from the very bright central source. The observations do show some filamentary structure with a similar morphology to that observed at 8 μm with IRAC.

3. The IRS spectrum of the low-mass protostar HH 46 IRS 1 displays many features common to those observed in high-mass protostars, e.g., the deeply embedded W33A source (Gibb et al. 2004). Thus, perhaps surprisingly, the different length scales and timescales, radiation fields, and outflow activity between low- and high-mass protostars have not produced a different global ice composition. The material in the envelope is well shielded from the outflow shocks and the stellar radiation entering the cavity.

4. The IRS spectrum of the fast-moving bow shock HH 47A is rich in strong forbidden emission lines at longer wavelengths (>15 μm) but, given the nature of the observations, at shorter wavelengths displays a series of weak H_2 and PAH emission features, which are likely to arise either at the edge of the wall of the cavity drilled by the bow shock or at the interface between the bow shock and the cloud.

We thank the referee for her/his useful comments and questions. This work is based on observations made with the *Spitzer Space Telescope*, which is operated by the Jet Propulsion Laboratory (JPL), California Institute of Technology, under NASA contract 1407 and contract 1224608 from JPL to the University of Texas. A. N.-C.'s research was partially supported by NASA-APD grant NRA0001-ADP-096.

REFERENCES

Adams, F. C., Lada, C. J., & Shu, F. H. 1987, ApJ, 312, 788
Boogert, A., et al. 2004, ApJS, 154, 359
Bregman, J. D., Hayward, T. L., & Sloan, G. C. 2000, ApJ, 544, L75
Cabrit, S., et al. 1999, in The Universe as Seen by *ISO*, ed. P. Cox & M. F. Kessler (ESA SP-427; Noordwijk: ESA), 449
Chernin, L. M., & Masson, C. R. 1991, ApJ, 382, L93
Correira, J. C. 2000, Ph.D. thesis, Queen Mary and Westfield College, Univ. London
Curiel, S., et al. 1995, ApJ, 453, 322
Demyk, K., Jones, A. P., Dartois, E., Cox, P., & D'Hendecourt, L. 1999, A&A, 349, 267
Dopita, M. A., Evans, I., & Schwartz, R. D. 1982, ApJ, 263, L73
Eislöffel, J., Davis, C. J., Ray, T. P., & Mundt, R. 1994, ApJ, 422, L91
Eislöffel, J., & Mundt, R. 1994, A&A, 284, 530
Emerson, J. P., et al. 1984, ApJ, 278, L49
Fazio, G., et al. 2004, ApJS, 154, 10
Gibb, E. L., Whittet, D. C. B., Boogert, A. C. A., & Tielens, A. G. G. M. 2004, ApJS, 151, 35
Gibb, E. L., et al. 2000, ApJ, 536, 347
Heathcote, S., et al. 1996, AJ, 112, 1141
Houck, J., et al. 2004, ApJS, 154, 18
Kaufman, M. J., & Neufeld, D. A. 1996, ApJ, 456, 611
Keane, J. V., et al. 2001, A&A, 376, 254
Kemper, F., et al. 2004, ApJ, 609, 826
Lefloch, B., Cernicharo, J., Cabrit, S., Noriega-Crespo, A., Moro-Martin, A., & Cesarsky, D. 2003, ApJ, 590, L41
Micono, M., Davis, C. J., Ray, T. P., Eislöffel, J., & Shetrone, M. D. 1998, ApJ, 494, L227
Molinari, S., & Noriega-Crespo, A. 2002, AJ, 123, 2010
Molinari, S., et al. 2000, ApJ, 538, 698
Moro-Martin, A., Noriega-Crespo, A., Molinari, S., Testi, L., Cernicharo, J., & Sargent, A. 2001, ApJ, 555, 146
Morse, J., Hartigan, P., Heathcote, S., Raymond, J. C., & Cecil, G. 1994, ApJ, 425, 738
Nisini, B. 2003, Ap&SS, 287, 207
Noriega-Crespo, A. 2002, Rev. Mex. AA Ser. Conf., 13, 71
Olberg, M., Reipurth, B., & Booth, R. S. 1992, A&A, 259, 252
Raga, A. C., & Cabrit, S. 1993, A&A, 278, 267
Raga, A. C., Noriega-Crespo, A., Gonzalez, R. F., & Velázquez, P. F. 2004, ApJS, 154, 346
Raymond, J. C., Morse, J. A., Hartigan, P., Curiel, S., & Heathcote, S. 1994, ApJ, 434, 232
Reipurth, B., & Heathcote, S. 1991, A&A, 246, 511
Rieke, G., et al. 2004, ApJS, 154, 25
Rosenthal, D., Bertoldi, F., & Drapatz, S. 2000, A&A, 356, 705
Schutte, W. A., & Khanna, R. K. 2003, A&A, 398, 1049
Schutte, W. A., et al. 1996, A&A, 315, L333
Schwartz, R. D. 1977, ApJ, 212, L25
Schwartz, R. D., & Greene, T. P. 2003, AJ, 126, 339
Shu, F. H., Najita, J., Ostriker, E. C., & Shang, H. 1995, ApJ, 455, L155
Stanke, T., McCaughrean, M. J., & Zinnecker, H. 1999, A&A, 350, L43

FIG. 1.—*Spitzer* image of the HH 46/47 system arising from the Bok globule (ESO 210-6A) obtained with IRAC. The color scheme is the following: *blue*, 3.6 μm; *green*, 4.5 + 5.8 μm; *red*, 8.0 μm. The image covers a region of $\sim 6.'5 \times 10.'6$, and in here the outflow is depicted at position angle of $\sim 30^{\circ}$.

PLATE 1

FIG. 4.—Combined three-color image of HH 46/47 using IRAC 4.5 μm (*blue*) and 8.0 μm (*green*) plus MIPS 24 μm (*red*). The apices of the HH 47A and 47C bow shocks are detected at 24 μm as well as the disruption of the Bok globule by the southwest outflow lobe. The HH 46 IRS central source produces a "banding effect" (the bright band) in IRAC channel 4. The image covers a region of $\sim 3' \times 5'$. North is up, and east is to the left.